

Article

Evapotranspiration in the Nile Basin: Identifying Dynamics and Drivers, 2002–2011

Henok Alemu ^{1,*}, Armel T. Kaptué ¹, Gabriel B. Senay ^{1,2,3}, Michael C. Wimberly ¹ and Geoffrey M. Henebry ¹

¹ Geospatial Sciences Center of Excellence (GSCE), South Dakota State University, Brookings, SD 57007, USA; E-Mails: armel.kaptue@sdsu.edu (A.T.K.); senay@usgs.gov (G.B.S.); michael.wimberly@sdsu.edu (M.C.W.); geoffrey.henebry@sdsu.edu (G.M.H.)

² Earth Resources Observation and Science (EROS) Center, U.S. Geological Survey, Sioux Falls, SD 57198, USA

³ North Central Climate Science Center (NC CSC), Colorado State University, Fort Collins, CO 80523, USA

* Author to whom correspondence should be addressed; E-Mail: henok.alemu@sdsu.edu; Tel.: +1-605-688-6591; Fax: +1-605-688-5227.

Academic Editor: Y. Jun Xu

Received: 9 February 2015 / Accepted: 1 September 2015 / Published: 9 September 2015

Abstract: Analysis of the relationship between evapotranspiration (ET) and its natural and anthropogenic drivers is critical in water-limited basins such as the Nile. The spatiotemporal relationships of ET with rainfall and vegetation dynamics in the Nile Basin during 2002–2011 were analyzed using satellite-derived data. Non-parametric statistics were used to quantify ET-rainfall interactions and trends across land cover types and subbasins. We found that 65% of the study area (2.5 million km²) showed significant ($p < 0.05$) positive correlations between monthly ET and rainfall, whereas 7% showed significant negative correlations. As expected, positive ET-rainfall correlations were observed over natural vegetation, mixed croplands/natural vegetation, and croplands, with a few subbasin-specific exceptions. In particular, irrigated croplands, wetlands and some forests exhibited negative correlations. Trend tests revealed spatial clusters of statistically significant trends in ET (6% of study area was negative; 12% positive), vegetation greenness (24% negative; 12% positive) and rainfall (11% negative; 1% positive) during 2002–2011. The Nile Delta, Ethiopian highlands and central Uganda regions showed decline in ET while central parts of Sudan, South Sudan, southwestern Ethiopia and northeastern Uganda showed increases. Except for a decline in

ET in central Uganda, the detected changes in ET (both positive and negative) were not associated with corresponding changes in rainfall. Detected declines in ET in the Nile delta and Ethiopian highlands were found to be attributable to anthropogenic land degradation, while the ET decline in central Uganda is likely caused by rainfall reduction.

Keywords: evapotranspiration; precipitation; vegetation; NDVI; land cover; trend analysis; Nile Basin

1. Introduction

Terrestrial evapotranspiration (ET)—the water transferred from the soil-plant complex to the atmosphere—plays an important role in water and energy budgets [1]. Next to precipitation, ET constitutes the largest component of the terrestrial water budget [2]. About three-fifths of the net solar radiation absorbed by earth's surface is used in ET and the accompanying sensible heat flux [3]. Characterizing the variation of terrestrial ET is also a key issue for understanding terrestrial components of the global water cycle given that about 40% of terrestrial precipitation originates from terrestrial ET; while about 57% of all terrestrial ET returns as terrestrial precipitation [4]. Consequently, accurate estimates of ET are key environmental constraints for climate and hydrological simulations [5–7], and for ensuring sustainable use of water resources [5,8] and hence the ability of biological systems to support human needs. This is especially true in the Nile Basin (Figure 1), a highly populated region in northeastern Africa, where surface water primarily originates from rainfall over an area encompassing about 25% of the Basin, with substantial parts of the Basin (about 40%) remaining water-limited and dependent on the Nile River for irrigation. The vulnerability of the Nile Basin region to climate [9] and land use [10,11] change and the responses of the hydrological cycle to these changes remain poorly understood.

Several studies have investigated the links between vegetation, ET and climate in Africa [10–19]. For instance, Jung *et al.* [12] analyzed long-term *in situ*, remote sensing and meteorological measurements, and attributed decreasing trends in ET in East Africa from 1998–2008 to decreasing trends in soil moisture. Marshall *et al.* [19] analyzed 31 years of trends in ET with trends in rainfall and surface temperature using remote sensing and surface climate reanalysis data; and suggested observed declines in ET in the Ethiopian highlands could be attributable to over-cultivation leading to land degradation. Pricope *et al.* [10] studied the spatial relationships between climate, vegetation change, degradation and population density in the East African Horn. Using the parametric statistical approach of linear regression trend tests with annual data, Alemu *et al.* [20] also detected declining ET trends in central portions of Uganda, eastern Sudan and Ethiopian highlands, but did not attempt to relate these trends directly to drivers. Other researchers found that both climatic and anthropogenic factors influence vegetation dynamics and thereby ET in east Africa [10,11]. Nonetheless, the interactions between ET and climatic drivers in Africa remain relatively unexplored [19].

Access to sufficiently reliable and consistent *in situ* hydrological data in the Nile Basin remains a major challenge [21], despite the monumental need to accurately assess and monitor the limited water and land resources in the Basin, and the growing demand for water from an increasing population. However, the availability of long-term, basin-wide temporally and spatially consistent remote sensing

data provides an opportunity to consistently and reliably provide geophysical and land resource data in a geographically comprehensive manner. Remote sensing provides the only feasible means to estimate ET over larger regions [2]. In addition, the reliability of remote sensing data for accurately estimating spatially explicit hydrological and biophysical data has improved significantly [21] to the extent that they can be used with confidence for water accounting and hydrological modeling, with overall accuracies of 95% for ET, 82% for rainfall, and 85% for land use [22]. Here we use publicly-available satellite-derived ET, rainfall, vegetation index, and land cover data to analyze ecohydrological dynamics and interrelationships in the Nile Basin during 2002 to 2011.

We analyzed the monthly relationship between ET and rainfall and examined how this relationship was influenced by land cover/land use in the Basin during the period from 2002 through 2011. For this analysis, we estimated per-pixel correlations at 1-km spatial resolutions between monthly time series of ET and rainfall and compared the results by land cover and subbasins. In order to evaluate the influence of rainfall and anthropogenic factors on changes in ET, we restricted our analysis to spatial associations of trends in rainfall and NDVI with corresponding trends in ET in the vegetated parts of the basin. For the spatiotemporal analysis we assessed pixel-scale temporal trends in ET, rainfall and vegetation greenness, spatially synthesized individual trends, and analyzed the relationships. Our objective was to address the following questions: (1) How are monthly ET dynamics related to rainfall in the Nile Basin? (2) How does this relationship vary with land cover? (3) What are the geographic extents and patterns of trends the Basin exhibited by ET, rainfall and vegetation dynamics? (4) Which regions exhibited change in ET as a result of rainfall-driven or anthropogenic factors?

2. Materials and Methods

2.1. Static Data

2.1.1. Study Area

The Nile Basin (Figure 1) is a major river basin in northeastern Africa and is drained by the longest river in the world. Home to 238 million people and shared by eleven countries, the basin traverses an extremely wide band of latitude from 4° S to 32° N. Its geographic location and latitudinal extent lead to a pronounced north-south rainfall gradient that divides the basin into three main rainfall regimes: arid, tropical and equatorial [23] with a corresponding gradient of vegetation productivity (Figure 1b).

Total basin area is ~3.7 million km². A water mask was used to exclude major water bodies of the basin (including Lakes Victoria, Albert, Tana, Kyoga, Edward) that constitute ~3% of the entire basin area. As this study is primarily a comparison of an operational ET product (SSEBop) with other datasets, a mask was generated for ET pixels with 0% frequency 8-day time series during the study period. Additionally, a mask was also generated for non-vegetated portions of the basin which corresponds to pixels with median of positive NDVI < 0.12 during 2002–2011 (*cf.* Figure 1b). The non-vegetated area mask covered nearly one-third (29%) of the entire basin area. The remaining unmasked 2.5 million km² of vegetated land surface comprised the study area.

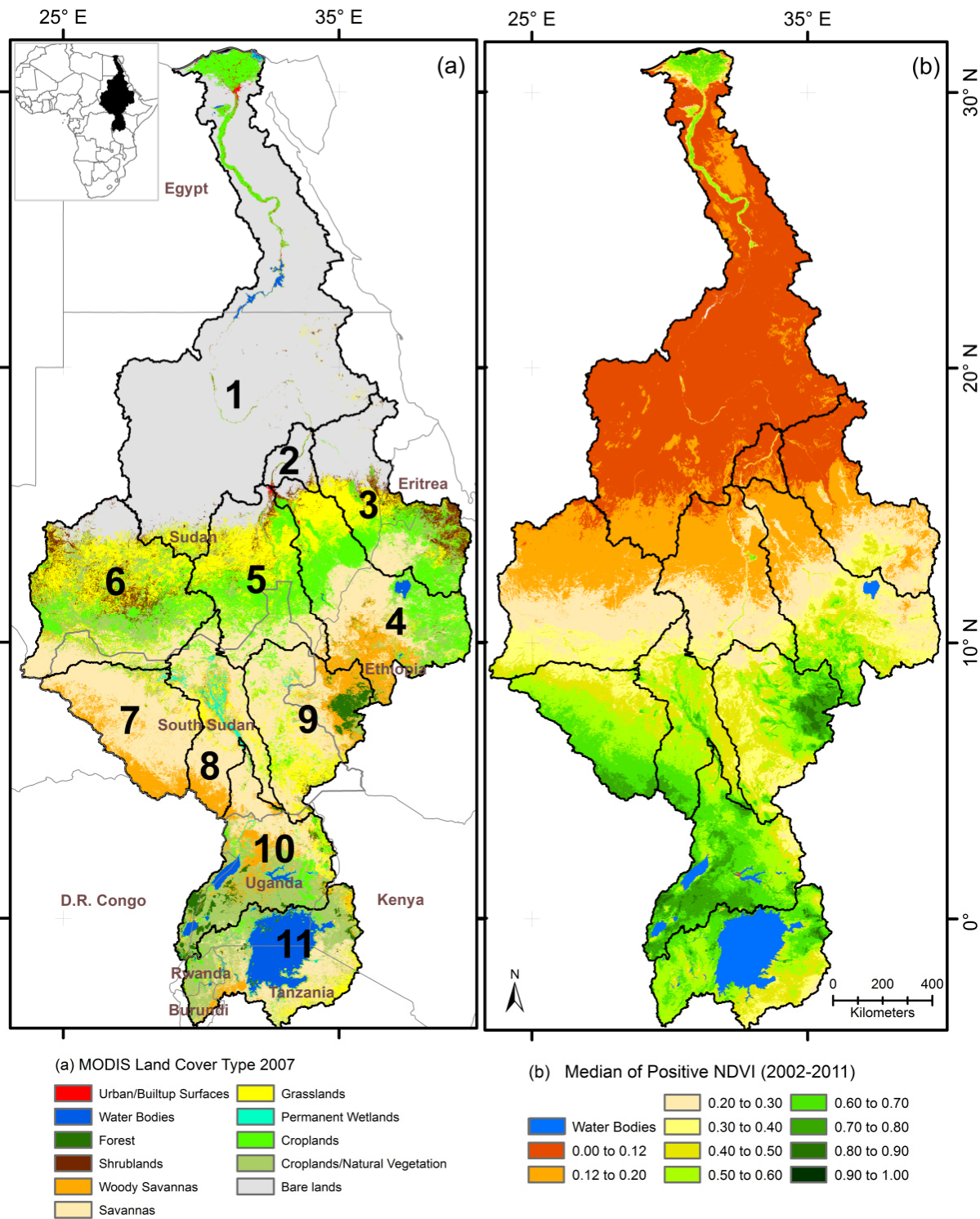


Figure 1. Nile Basin. (a) MODIS land cover map (MCD12Q1, IGBP scheme) for the year 2007 [24]; (b) Median of positive NDVI values for the period of 2002–2011 derived from time series of MODIS NBAR (MCD43B4) [25] composite data. Black lines show subbasin boundaries; grey lines show country boundaries; numbers show subbasin ID.

2.1.2. Land Cover

The Moderate Resolution Imaging Spectroradiometer (MODIS) land cover type product (MCD12Q1) is a global map of land cover types derived using observations collected by the MODIS sensors onboard

the Aqua and Terra satellites [24]. It is produced at annual time steps with a spatial resolution of 500 m and comes in five different classification schemes. We used the 2007 land cover product with the International Geosphere Biosphere Programme (IGBP) classification scheme, which contains 17 land cover classes, as representative of the study period (2002–2011). The 16 land cover units found in the Nile Basin (Figure 1a) were thematically aggregated into 9 major land cover classes, *viz.*, (1) Croplands; (2) Croplands and Natural Vegetation mosaic (CNV); (3) Forest; (4) Savannas; (5) Woody Savannas; (6) Shrublands; (7) Grasslands; (8) Permanent wetlands; and (9) Bare Lands. We synthesized two new land cover classes (i) Forest, by aggregating 5 IGBP classes (Evergreen Needleleaf Forest, Evergreen Broadleaf forest, Deciduous Needleleaf Forest, Deciduous Broadleaf Forest, Mixed Forest) and (ii) Shrublands (Closed Shrublands and Open Shrublands). The resulting land cover map (Figure 1a) was resampled to 1-km to match the spatial resolution of ET and vegetation data using the majority class filter as described in Kaptué *et al.* [26]. Our data encompassed 10 MODIS tiles (h20v05-09 and h21v05-09), which were acquired from Reverb, a metadata and service discovery tool [27].

2.1.3. Basin Delineation Data

Vector data (ESRI shape file) for the basin delineation were acquired from U.S. Geological Survey (USGS) HYDROSHEDS (HYDROlogical data and maps based on SHuttle Elevation Derivatives at multiple Scales) 15-s data [28]. Vector data for delineation of major subbasins and inland water bodies were acquired from the FAO GeoNetwork Database [29]. The 11 major subbasins (Figure 1) and their proportional area with respect to the entire basin area (3.7 million km²) are as follows: (1) Main Nile Khartoum (27%); (2) Main Nile Atbara (1%); (3) Atbara (7%); (4) Blue Nile (10%); (5) White Nile (8%); (6) Bahr el-Arab (12%); (7) Bahr el-Ghazal (6%); (8) Sudd (5%); (9) Sobat (7%); (10) Aswa (8%); and (11) Victoria (8%).

2.2. Time Series Data

2.2.1. Evapotranspiration Data

The monthly Operational Simplified Surface Energy Balance (SSEBop) ET product [30] at 1-km spatial resolution (Figure 2b shows mean annual ET average for 2002–2011) was acquired from the USGS Earth Resources Observation and Science (EROS) Center. The SSEBop is an operational parameterization of the Simplified Surface Energy Balance (SSEB) model [31]. It uses MODIS-derived land surface temperature and model-assimilated meteorological data to generate a gridded ET product [30].

2.2.2. Precipitation Data

Daily rainfall data were obtained from the Tropical Rainfall Measuring Mission (TRMM) at 0.25° spatial resolution between 2002 and 2011 (product 3B42, version 7) [32]. The daily data (in mm/day) were temporally aggregated to monthly time series and resampled to 1-km spatial resolution using bilinear interpolation technique to match the spatial resolution of ET and vegetation data. The data were acquired from NASA's TRMM webpage [33]. Figure 2a presents rainfall distribution across the basin using mean annual rainfall during 2002–2011. Moreover, the difference between rainfall and ET showing key water source and sink areas is shown in Figure 2c.

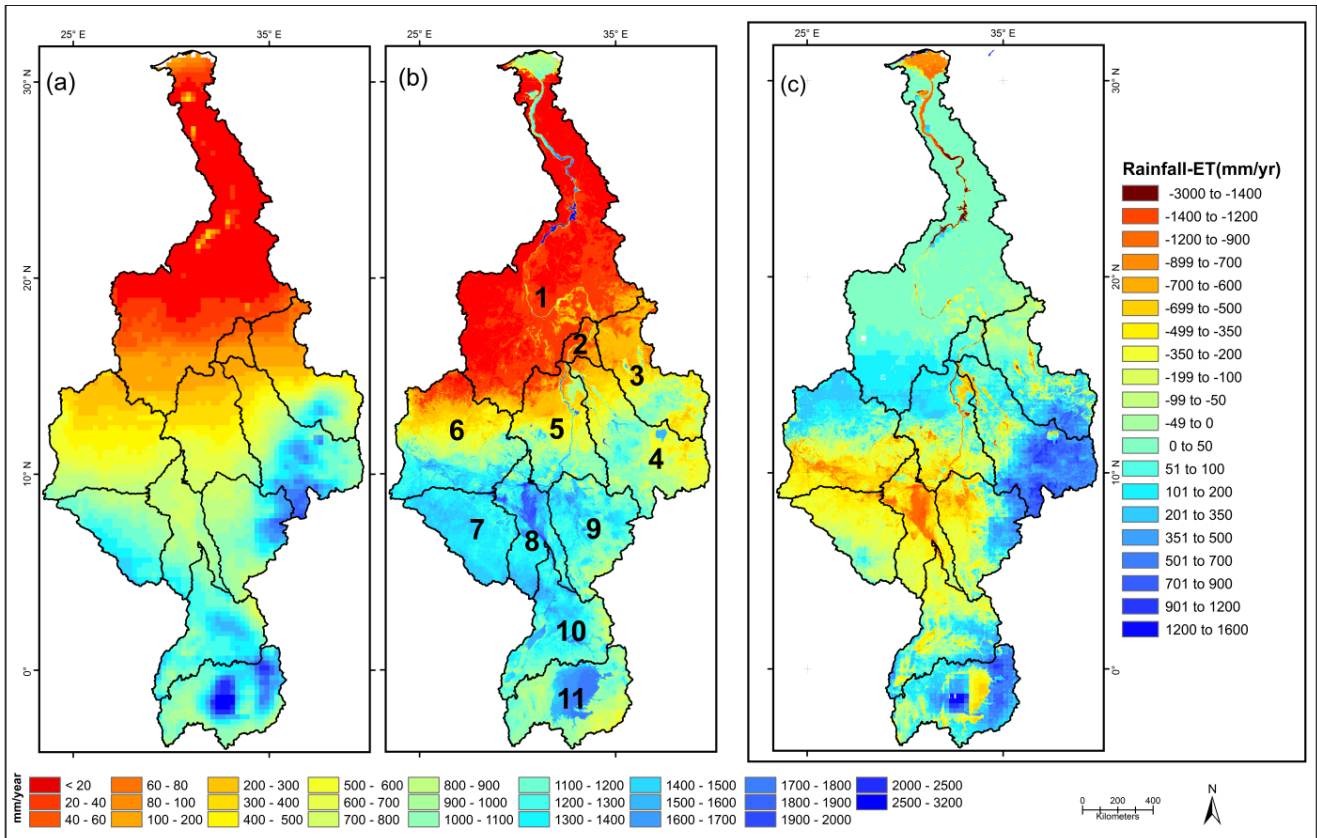


Figure 2. Nile Basin. (a) Annual rainfall (TRMM, 2002–2011); (b) Annual ET (SSEBop, 2002–2011); and (c) Rainfall-ET (2002–2011). Black lines show subbasin boundaries; numbers show subbasin ID.

2.2.3. Vegetation Data

As a proxy for vegetation productivity, the Normalized Difference Vegetation Index (NDVI) data were generated from the MODIS nadir bidirectional reflectance distribution function (BRDF) adjusted reflectance (NBAR) product (MCD43B4) [25]. The NDVI was calculated for each 16-day NBAR composite (updated every 8 days) as the ratio of the difference between the near-infrared (0.841–0.876 μm) and red (0.620–0.670 μm) bands normalized by the sum of the two bands. A monthly time series of NDVI data was then compiled using the maximum composited NDVI for each month during 2002–2011. The 10 MODIS NBAR tiles (h20v05-09 and h21v05-09) were acquired from Reverb, a metadata and service discovery tool [27].

2.3. Statistical Analysis

2.3.1. Correlation Analysis

To investigate the interactions between rainfall and ET from 2002 to 2011, nonparametric Kendall rank correlations [34,35] between monthly time series data of ET and rainfall were calculated and tested against the null hypothesis that the correlation values were not significantly different from zero. To analyze the relationship between land cover and ET-rainfall interactions, the median of ET-rainfall correlations were calculated for individual land cover classes in all subbasins.

2.3.2. Trend Analysis

The nonparametric Seasonal Mann-Kendall trend test (SMK) [34–36] was applied to each of the three time series (ET, rainfall, and NDVI). For each time series, the resulting SMK statistic and associated p -value maps were combined to produce a three-class map (Positive (p), Negative (n), Not Significant (o)) at three significance levels: $p < 0.05$, $p < 0.01$ and $p < 0.001$.

To attenuate noise and remove individual outlier pixels, a 3×3 median filter was applied to both correlation (Figure 3) and trend maps (Figure 5). The Kendall rank correlations and SMK tests were performed using Kendall library [34] in the R software environment [37].

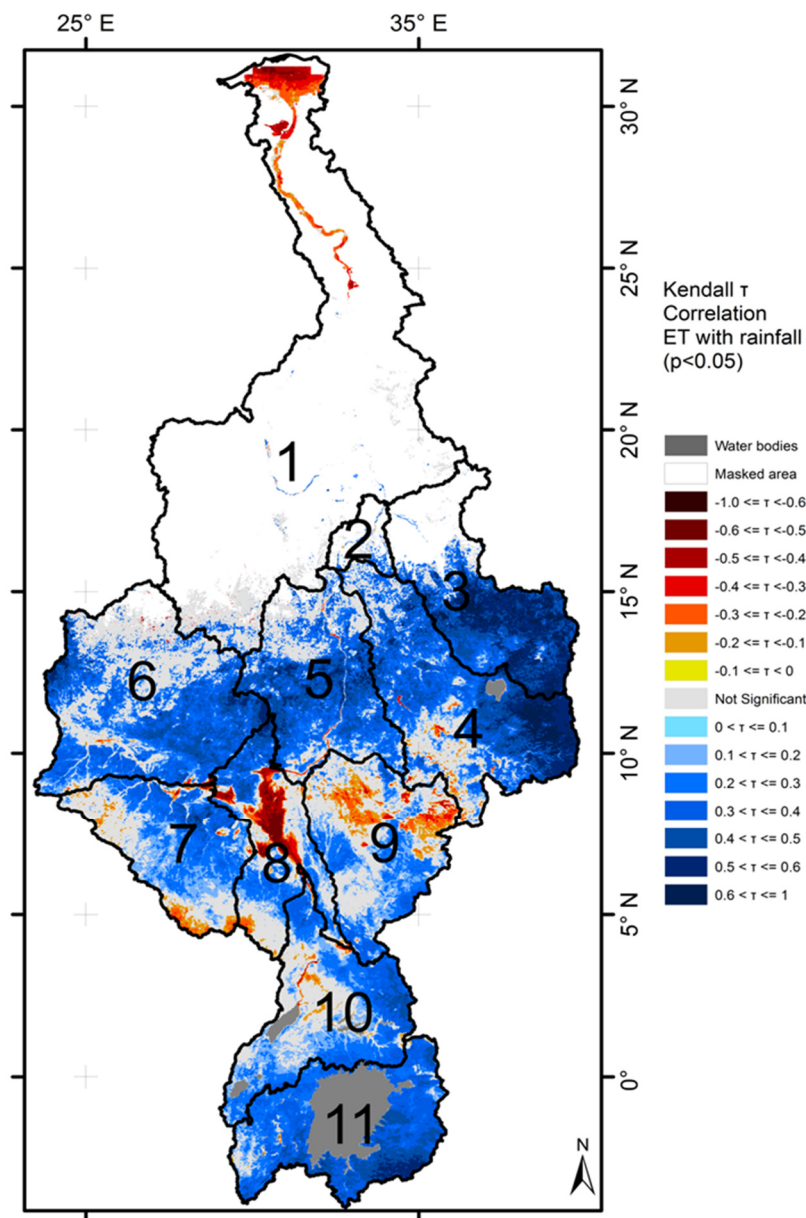


Figure 3. Spatial distribution of Kendall rank correlation coefficients (τ) between monthly time series of ET and rainfall. Displayed correlation coefficients are statistically significant ($p < 0.05$). Data used are positive values of SSEBop ET [30] and TRMM rainfall [32] at spatial resolution of 1-km. Numbered polygons are major subbasins of the Nile. Major water bodies are shown in grey.

2.3.3. Synthesis of Trends

Spatial association between the trend maps were used to evaluate how trends of ET were associated with trends of rainfall and NDVI. To analyze how changes in ET associate with significant changes and/or no-changes in rainfall and NDVI, we combined the two trend categories of ET (positive and negative, $p < 0.05$) with three trend categories of rainfall and NDVI (Positive, Negative, Not Significant classes, $p < 0.05$) and generated a geodatabase with 18 classes (Table 1).

Table 1. Table showing synthesis of SMK trends ($p < 0.05$) of monthly ET, rainfall and monthly maximum NDVI. The 18-classes encode the combined trends in ET-rainfall-NDVI order.

ET-Rainfall-NDVI Trend Synthesis (1st–2nd–3rd)				
Rainfall (2nd order)	NDVI (3rd order)	ET (1st order)		
		p	n	
p	p	ppp	npp	
	o	ppo	npo	
	n	ppn	npn	
o	p	pop	nop	
	o	poo	noo	
	n	pon	non	
n	p	pnp	nnp	
	o	pno	nno	
	n	pnn	nnn	

Notes: p-positive; n-negative; o-not significant.

3. Results and Discussion

3.1. Temporal Correlations across Space

Figure 3 illustrates the spatial distribution of the Kendal tau (τ) rank correlation coefficients between monthly time series of ET and rainfall from 2002 through 2011. The dominance of statistically significant ($p < 0.05$) positive τ -values, covering about two-thirds of the study area, strengthens the conclusions from earlier reports that showed that rainfall is the key driver of seasonal and interannual variability in ET in the region [12,20,38]. About 28% of the study area (2.5 M·km²) showed no statistically significant relationship.

Areas with relatively strong positive correlations (light blue to dark blue) were observed stretching across the Sahelian belt (10° N to 15° N) from western Sudan to Ethiopian highlands (subbasins 3–6). This pattern agrees with the consensus that rainfall is the dominant limiting factor on semi-arid vegetation growth and ET [13,38–40]. Farther south, a diagonal band of positive correlation pixels was identified stretching from southwestern South Sudan (subbasin 7) to northeastern Uganda (subbasin 10). The southern portions of the basin surrounding Lake Victoria (subbasins 10 and 11), a region characterized by wetter climate, also showed positive correlation pixels.

Areas with negative correlations (yellow to dark-red, Figure 3) constituted ~7% of the study area. In subbasin 1, the Nile delta and valley in Egypt exhibited relatively strong negative correlations ($-0.5 \leq \tau < -0.2$). This pattern occurs because the Nile delta and valley are intensively irrigated

agricultural regions [41] in an arid climate with very limited rainfall [20,23]. Crop productions in those regions are almost wholly dependent on irrigation from the Nile River [41,42].

3.2. Land Cover-ET-Rainfall Relationships

The color-coded matrix in Figure 4 shows ET-rainfall correlation coefficients with respect to land cover types for each of the eleven subbasins. Negative correlation coefficients were the results of the land cover decoupling the local effects of precipitation on ET, through the provision of an alternate source of water to supply ET demands. On the other hand, the interaction remained positive when there is little or no influence of land cover.

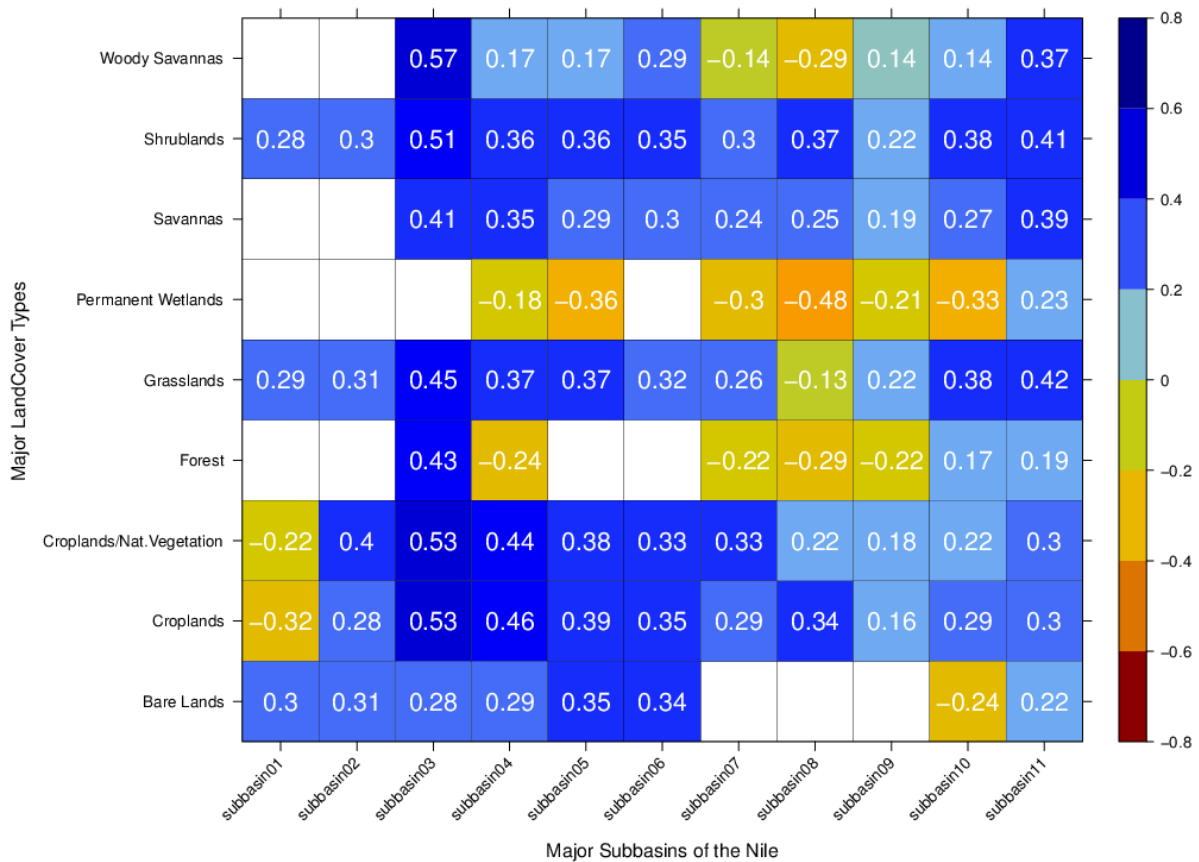


Figure 4. Color-coded matrix displays statistically significant ($p < 0.05$) Kendall tau (τ) rank correlation coefficients between ET and rainfall averaged by land cover type for the 11 major subbasins of the Nile basin. Colors range from dark-red (for strongly negative) to dark-blue (for strongly positive) correlations. A 3×3 majority filter was applied on the land cover map. Empty boxes indicate an absence of the land cover type in the subbasin.

Land cover types that exhibited positive ET-rainfall interactions included natural vegetation types (shrublands, savannas, grasslands and woody savannas), CNV, croplands, and bare lands. In subbasins that have wetter hydro-climatic characteristics such as subbasin 8, where moisture availability is supplied by sources other than rainfall (e.g., wetlands, soil moisture or base flow), woody savanna and grasslands exhibited negative ET-rainfall relationships. Negative correlations observed over CNV and croplands in subbasin 1 resulted from the subbasin being almost entirely irrigated as rainfall is negligible.

3.3. Temporal Dynamics

Seasonal Mann-Kendall (SMK) trend results for monthly time series of ET, rainfall and monthly-maximum NDVI data during 2002–2011 are presented in Figure 5 at three different significance levels (0.05, 0.01 and 0.001).

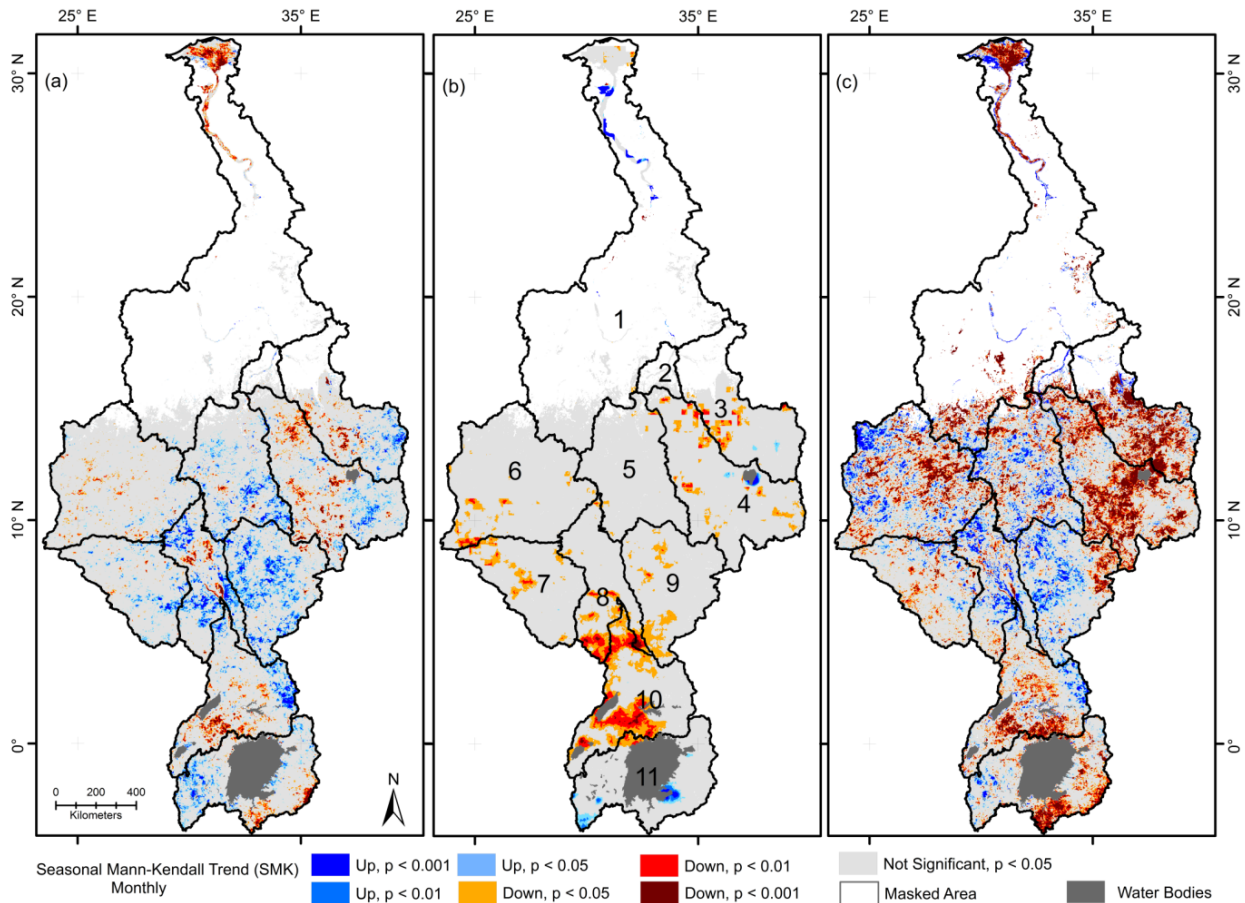


Figure 5. Maps of statistically significant Seasonal Mann-Kendall trends of (a) ET; (b) Rainfall; and (c) NDVI for the period between 2002 and 2011 using monthly time series of monthly ET, monthly rainfall, and monthly maximum NDVI at 1-km spatial resolution.

3.3.1. ET Patterns

The extent of statistically significant trends in ET detected in the basin was limited, with just 12% and 6% of the unmasked area showing positive and negative ET changes, respectively, at a p -value of 0.05 or less (Figure 5a). The central regions of the basin in parts of Sudan and South Sudan (subbasins 5,8,9) showed an overall positive change in ET. In addition, small pockets of positive ET changes were identified in eastern Ethiopian highlands (subbasins 3,4), northeastern Uganda (subbasin 10) and Rwanda/Burundi regions (subbasin 11). The ET trends in the inland portions of the Nile delta and Nile valley in subbasin 1 were negative (Figure 5a), in contrast with the positive ET trends detected on the fringes of the delta. In addition, smaller spots of negative ET trends were detected in eastern Sudan (subbasins 3,4), the western Ethiopian highlands (subbasins 3,4), in regions surrounding the Sudd Wetlands in South Sudan (subbasin 8), central Uganda (subbasin 10) and Tanzania (subbasin 11) regions. The declines in ET in the Ethiopian

highlands were in agreement with the findings of Marshall *et al.* [19]. As the significance levels are tightened, the corresponding areas of positive and negative trends contract. Positive trends occurred at 5% and 2% for $p < 0.01$ and $p < 0.001$, respectively; whereas, negative trends occurred at 3% and 1% for $p < 0.01$ and $p < 0.001$, respectively.

Significant declines in ET in the agricultural lands of the Nile delta and valley in Egypt have been observed in subbasin 1. This was likely caused by a combination of man-made land degradation (chemical and physical) that occurred in the delta. Several researchers have reported soil degradation through increased soil salinization as a result of saline drainage water reuse for irrigation [43–45]. Moreover, some portions of the delta also exhibited physical land degradation from urban land encroachment on agricultural areas [46,47]. However, the fringes of the Nile delta showed increases in ET, which were likely a consequence of expanding irrigation in newly reclaimed agricultural lands [48–50].

3.3.2. Rainfall Patterns

The results of the monthly rainfall trend analysis over 10 years in Figure 5b showed that substantial parts (88%) of the unmasked area experienced no statistically significant ($p < 0.05$) change. However, 11% and 3% of the area were characterized by declines in rainfall at the 0.05 and 0.01 significance levels respectively. The most conspicuous regions where rainfall declines were detected include along the Uganda-South Sudan border (subbasins 8 and 10), and in central Uganda, north of Lake Victoria (subbasin 10). In general, the rainfall dynamics in the basin during 2002–2011 showed no trends, but given high interannual variation in timing of rainfall [51], the length of the period examined was likely too short to reveal significant trends.

These observations in rainfall trends in the basin were also reported by Alemu *et al.* [20] who used linear regression to detect trends in annual rainfall using TRMM data (2002–2011). They found large-scale reductions in rainfall in South Sudan-Uganda border (subbasins 8 and 10), central Uganda (subbasin 10) and eastern Sudan (subbasin 3 and 4). A recent study by Hoscilo *et al.* [11] who also used linear regression to detect trends in annual rainfall (FEWSNET RFE 2.0 data for 2001–2010) also confirmed declines in rainfall across large swaths of central Uganda (subbasin 10). However, our results largely diverge from the Hoscilo *et al.* [11] findings. Our results indicate no part of the unmasked area exhibited increase in rainfall with the exception of few pixels bordering Lake Tana and Lake Victoria. Other researchers using gauge data also found no signs of recent rainfall trends in eastern parts of subbasin 4 [52,53].

3.3.3. Vegetation Patterns

The NDVI trend map generated using the monthly maximum NDVI time series (Figure 5c) showed that a sizeable 36% of the study area exhibited statistically significant ($p < 0.05$) changes—12% positive and 24% negative in vegetative greenness. The affected area was 7% (4%) positive and 16% (10%) negative at $p < 0.01$ ($p < 0.001$).

The Ethiopian highlands covering subbasins 3 and 4 exhibited the most geographically contiguous decline in vegetative greenness. This pattern agrees with Pricope *et al.* [10] who found declining trends in NDVI in Ethiopia during 1999–2011. Considerable vegetative decline was detected in the Nile delta/valley regions in subbasin 1 while both sides of the fringes of the Nile delta exhibited increasing

greenness and much of the inland delta exhibited declines. The changes in vegetative greenness in the Nile delta and valley followed similar patterns as the ET changes. Increases in greenness in the fringes of the delta are indicators of the expansion of irrigation activities in areas that were initially bare lands. The decline in greenness in the inland parts of the delta may result from a combination of anthropogenically-induced chemical (soil salinity) and physical (loss of agricultural fields) land degradation caused by irrigation by reuse of saline drainage water, population pressure leading to loss of agricultural fields to urban sprawl [43–47].

Regions of central Uganda (subbasin 10), south of Lake Victoria in Tanzania (subbasin 11) and western (subbasin 6) and eastern (subbasins 3 and 4) Sudan also exhibited vegetative declines. The regions with a significantly positive NDVI trend were mainly located in the central parts of the basin (subbasins 5,8,9), and also in smaller pockets in western Sudan (subbasin 6) and northeastern Uganda (subbasin 10).

3.4. Synthesis of Individual Trends

Using individual trends in ET, rainfall and NDVI, we synthesized 18 combinations (Table 1) of trends for regions where significant changes in ET were detected. The geographic extent of synthesized combination of trends spanned over an area of 0.5 M km² or nearly one-fifth of the unmasked area. Positive ET changes represented about two-thirds (~33.5 thousand km²) of this area, while the remaining one-third (~17.7 thousand km²) were negative. Only five of the 18 classes constituted at least 1% of the total study area (~20 thousand km²) each. With respect to the trend direction in ET, these five classes can be placed into two groups: (1) where ET increases (*poo* & *pop*); and (2) where ET decreases (*non*, *noo* and *nnn*). Altogether, these two groups constituted 18% of the entire study area, and 88% of the area that exhibited changes in ET. The synthesis map of these 5 classes as Groups 1 and 2 revealed the distinct geographic distribution between the two groups across the basin (Figure 6).

Group 1 includes areas in which ET exhibited increasing trends with no trend in rainfall, and either no significant change in NDVI (*poo*) or a significant positive trend in NDVI (*pop*). Group 1 covers 14% of the study area and 57% of the areas that exhibited change in ET. Occurrences of Group 1 tended to cluster together and are largely located in the center of the Basin (subbasins 5,8,9) and, to a lesser extent, in northeastern part of subbasin 10 and western part of subbasin 11. ET increases in those regions are not associated with corresponding increases in rainfall.

Group 2 includes areas that exhibited significant negative trends in ET and constitutes about 7% of the study area or 31% of the area that exhibited ET changes. Both classes *non* and *noo* represent no trend in rainfall, while *non* represents downward trending NDVI as well. The third class in Group 2 covers areas in which significant decreasing trends were observed in ET, rainfall, and the NDVI. Group 2 conditions occurred in the Nile delta in subbasin 1, in eastern part of the study area in subbasins 3 and 4, and in regions north and south of Lake Victoria in subbasins 10 and 11 (Figure 6).

Almost the entire regions of the inland Nile delta (subbasin 1) were classified as *non*. As the delta is highly populated and intensively irrigated [41], the decline in ET and NDVI is the likely consequence of soil salinization (as saline drainage water is used for irrigation) and/or agricultural land degradation (as urban encroachment on agricultural fields) [46,47]. This is in contrast to the fringe regions of the delta that were classified as *pop*, indicating an increase in both ET and NDVI with no change in rainfall.

This finding in the peripheries of the delta is in agreement with other researchers who identified expansion of irrigation activity in newly reclaimed land in the fringes of the delta [48,49].

The decline in NDVI in association with the decline in ET (class *non*) was mainly observed in subbasins 3 and 4 and is likely caused by non-rainfall-driven land degradation. This non-rainfall-driven degradation in the Ethiopian highlands is likely from increasing population pressure and has been reported by other researchers [10,11,54]. On the other hand, class *noo* was mainly observed around the Sudd Wetlands in subbasin 8, and can be explained by the dynamics of wetland ecosystems where ET decline is independent of rainfall. Class *nnn* was observed in subbasin 10 north of Lake Victoria. A previous study also found linear trends of declining rainfall and ET in central parts of Uganda (subbasin 10) during 2002–2011 [20].

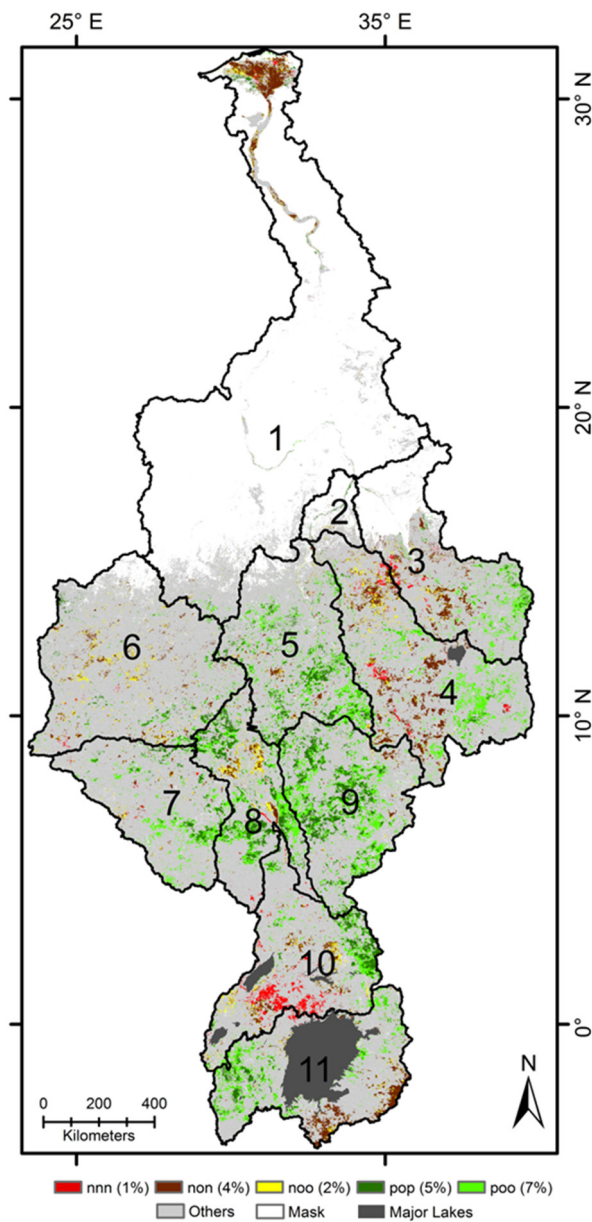


Figure 6. Per-pixel synthesis map of significant trends ($p < 0.05$) in ET, rainfall and NDVI with 5 major combination classes of trends. Gray areas represent regions that exhibit no significant trend in ET. The colored 5 major classes encoding the combined trends in ET-rainfall-NDVI order are shown with their proportional area with respect to study area.

4. Conclusions

We have explored seasonal ET dynamics as well as multiyear trends, attempting to understand the relationships between ET, rainfall and land cover both in terms of monthly variability as well as the changes that occurred over the period of 2002–2011. Results from monthly ET-rainfall correlations indicated that 65% of the basin showed positive relationships while only 7% showed negative. The semi-arid regions of the basin (Sahelian belt), large parts of the Ethiopian highlands, the regions surrounding Lake Victoria exhibited positive ET-rainfall relationships, as expected. On the other hand, the Nile valley and delta, the Sudd Wetlands and eastern South Sudan and southwestern Ethiopia exhibited negative ET-rainfall relationships. Analysis of the monthly ET-rainfall relationships with land cover showed that the relationship is generally negative over forests and wetlands; while it is positive in most subbasins over woody savannas, savannas, shrublands, and grasslands as well as anthropogenic land covers such as croplands and CNVs.

Analysis and synthesis of the trends in ET, rainfall and NDVI revealed that the inland parts of the Nile delta exhibited declines in ET and NDVI, possibly indicating soil salinization as a result of use of saline drainage water for irrigation and/or agricultural land degradation as a result of urban sprawl in the delta. In contrast, we found increasing trends in both ET and NDVI indicating signs of agricultural expansion and land reclamation in both fringes of the Nile delta. We have also revealed downward trends in ET and NDVI in the Ethiopian highlands where there has been no significant trend in rainfall. Since this is highly populated land with mainly rainfed subsistence agriculture, the decline in both ET and greenness is likely an indication of land degradation. Central parts of Uganda exhibited declining trends in ET and NDVI as well as in rainfall. These declines in both ET and NDVI are likely driven by associated decreases in rainfall. Large areas in the central part of the basin where increasing trends in ET and NDVI were observed were not associated with corresponding increasing trends in rainfall.

It should be noted that the relatively short-time period of the study (10 years) most likely captured the influences of short-term climatic variations rather than slower evolving dynamics resulting from global climate change. As a result, the trends documented in this study should not be extrapolated in to the future, but instead should be viewed as significant changes of historical fluctuations over the decade in climatic conditions and human land use. The various model-assimilated and satellite-derived data products used in the study, including ET, rainfall estimates, vegetation indices, land cover classification, as well as methods employed such as downscaling of rainfall data, all introduce levels of uncertainty, sometimes not well-characterized, that likely increased the noise in the data and limited our ability to detect relatively-short-term trends.

Despite these limitations, the study provides evidence that land use/land cover influence the association between local rainfall and ET and is a likely driver of short-term trends in ET throughout many parts of the basin. Continued basin-wide monitoring of hydrological processes and land use and land cover characteristics using satellite remote sensing will provide a basis for characterizing future changes and continuing to improve our understanding of the drivers of ET in the Nile Basin.

Acknowledgments

This work has been partially funded by NASA Applied Science Program contract# NNA06CH751 and by the Geospatial Sciences Center of Excellence (GSCE), South Dakota State University. Any use of trade, firm or product names is for descriptive purposes only and does not imply endorsement by the U.S. Government.

Author Contributions

Henok Alemu formulated the research problem. Henok Alemu and Armel T. Kaptué conceptualized the research design and implementation. Gabriel B. Senay, Michael C. Wimberly and Geoffrey M. Henebry revised the manuscript and provided thorough feedback. All authors contributed to the writing of the manuscript.

Conflicts of Interest

The authors declare no conflict of interest.

References

1. Wang, K.; Dickinson, R.E. A review of global terrestrial evapotranspiration: Observation, modeling, climatology, and climatic variability. *Rev. Geophys.* **2012**, *50*, doi:10.1029/2011RG000373.
2. Glenn, E.P.; Huete, A.R.; Nagler, P.L.; Hirschboeck, K.K.; Brown, P. Integrating remote sensing and ground methods to estimate evapotranspiration. *Crit. Rev. Plant. Sci.* **2007**, *26*, 139–168.
3. Trenberth, K.E.; Fasullo, J.T.; Kiehl, J. Earth's global energy budget. *Bull. Am. Meteorol. Soc.* **2009**, *90*, 311–323.
4. Van der Ent, R.J.; Savenije, H.H.G.; Schaefli, B.; Steele-Dunne, S.C. Origin and fate of atmospheric moisture over continents. *Water Resour. Res.* **2010**, *46*, W09525, doi:10.1029/2010WR009127.
5. Mu, Q.; Zhao, M.; Running, S.W. Improvements to a MODIS global terrestrial evapotranspiration algorithm. *Remote Sens. Environ.* **2011**, *115*, 1781–1800.
6. Bastiaanssen, W.; Perry, C. *Agriculture Water Use and Water Productivity in the Large Scale Irrigation Schemes of the Nile Basin*; Nile Basin Initiative: Entebbe, Uganda, 2009.
7. Mohamed, A.; van den Hurk, B.J.J.M.; Savenije, H.H.G.; Bastiaanssen, W.G.M. Impact of the Sudd Wetland on the Nile hydroclimatology. *Water Resour. Res.* **2005**, *40*, 1–14.
8. Fisher, J.B.; Whittaker, R.J.; Malhi, Y. ET come home: Potential evapotranspiration in geographical ecology. *Glob. Ecol. Biogeogr.* **2011**, *20*, 1–18.
9. Di Baldassarre, G.; Elshamy, M.; van Griensven, A.; Soliman, E.; Kigobe, M.; Ndomba, P.; Mutemi, J.; Mutua, F.; Moges, S.; Xuan, Y.; *et al.* Future hydrology and climate in the River Nile Basin: A Review. *Hydrol. Sci. J.* **2011**, *56*, 199–211.
10. Pricope, N.G.; Husak, G.; Lopez-Carr, D.; Funk, C.; Michaelsen, J. The climate-population nexus in the East African Horn: Emerging degradation trends in rangeland and pastoral livelihood zones. *Glob. Environ. Chang.* **2013**, *23*, 1525–1541.

11. Hoscilo, A.; Balzter, H.; Bartholomé, E.; Boschetti, M.; Brivio, P.A.; Brink, A.; Clerici, M.; Pekel, J.F. A conceptual model for assessing rainfall and vegetation trends in sub-Saharan Africa from satellite data. *Int. J. Clim.* **2014**, doi:10.1002/joc.4231.
12. Jung, M.; Reichstein, M.; Ciais, P.; Seneviratne, S.I.; Sheffield, J.; Goulden, M.L.; Bonan, G.; Cescatti, A.; Chen, J.; de Jeu, R.; *et al.* Recent decline in the global land evapotranspiration trend due to limited moisture supply. *Nature* **2010**, *467*, 951–954.
13. Fensholt, R.; Langanke, T.; Rasmussen, K.; Reenberg, A.; Prince, S.D.; Tucker, C.; Scholes, R.J.; Le, Q.B.; Bondeau, A.; Eastman, R. Greenness in semi-arid areas across the globe 1981–2007—An Earth Observing Satellite based analysis of trends and drivers. *Remote Sens. Environ.* **2012**, *121*, 144–158.
14. Anyamba, A.; Tucker, C.J. Analysis of Sahelian vegetation dynamics using NOAA-AVHRR NDVI data from 1981–2003. *J. Arid Environ.* **2005**, *63*, 596–614.
15. Herrmann, S.M.; Anyamba, A.; Tucker, C.J. Recent trends in vegetation dynamics in the African Sahel and their relationship to climate. *Glob. Environ. Chang.* **2005**, *15*, 394–404.
16. Huber, S.; Fensholt, R.; Rasmussen, K. Water availability as the driver of vegetation dynamics in the African Sahel from 1982 to 2007. *Glob. Planet. Chang.* **2011**, *76*, 186–195.
17. Zeng, N.; Neelin, J.D.; Lau, K.-M.; Tucker, C.J. Enhancement of interdecadal climate variability in the Sahel by vegetation interaction. *Science* **1999**, *286*, 1537–1540.
18. Seaquist, J.; Hickler, T.; Eklundh, L.; Ardö, J.; Heumann, B. Disentangling the effects of climate and people on Sahel vegetation dynamics. *Biogeosciences* **2009**, *6*, 469–477.
19. Marshall, M.; Funk, C.; Michaelsen, J. Examining evapotranspiration trends in Africa. *Clim. Dyn.* **2012**, *38*, 1849–1865.
20. Alemu, H.; Senay, G.; Kaptue, A.; Kovalsky, V. Evapotranspiration variability and its association with vegetation dynamics in the Nile Basin, 2002–2011. *Remote Sens.* **2014**, *6*, 5885–5908.
21. Bastiaanssen, W.; Karimi, P.; Rebelo, L.-M.; Duan, Z.; Senay, G.; Muthuwatte, L.; Smakhtin, V. Earth observation based assessment of the water production and water consumption of Nile Basin agro-ecosystems. *Remote Sens.* **2014**, *6*, 10306–10334.
22. Karimi, P.; Bastiaanssen, W. Spatial evapotranspiration, rainfall and land use data in water accounting—Part 1: Review of the accuracy of the remote sensing data. *Hydrol. Earth Syst. Sci. Discuss.* **2014**, *11*, 1073–1123.
23. Camberlin, P. Nile Basin Climates. In *The Nile: Origin, Environments, Limnology and Human Use*; Dumont, H.J., Ed.; Springer: Berlin, Germany, 2009; pp. 307–333.
24. Friedl, M.A.; Sulla-Menashe, D.; Tan, B.; Schneider, A.; Ramankutty, N.; Sibley, A.; Huang, X. MODIS Collection 5 global land cover: Algorithm refinements and characterization of new datasets. *Remote Sens. Environ.* **2010**, *114*, 168–182.
25. Schaaf, C.B.; Gao, F.; Strahler, A.H.; Lucht, W.; Li, X.; Tsang, T.; Strugnell, N.C.; Zhang, X.; Jin, Y.; Muller, J.-P. First operational BRDF, albedo nadir reflectance products from MODIS. *Remote Sens. Environ.* **2002**, *83*, 135–148.
26. Kaptué Tchuenté, A.T.; Roujean, J.-L.; De Jong, S.M. Comparison and relative quality assessment of the GLC2000, GLOBCOVER, MODIS and ECOCLIMAP land cover data sets at the African continental scale. *Int. J. Appl. Earth Obs. Geoinf.* **2011**, *13*, 207–219.

27. NASA's Next Generation Earth Science Discovery Tool (Reverb | Echo). Available online: reverb.echo.nasa.gov/reverb/ (accessed on 6 May 2014).
28. Lehner, B.; Verdin, K.; Jarvis, A. *HydroSHEDS Technical Documentation, Version 1.0*; World Wildlife Fund: Washington, DC, USA, 2006.
29. United Nations Food and Agriculture Organization (FAO). *GEONETWORK Data Portal*; FAO: Rome, Italy, 2013.
30. Senay, G.B.; Bohms, S.; Singh, R.K.; Gowda, P.H.; Velpuri, N.M.; Alemu, H.; Verdin, J.P. Operational Evapotranspiration Mapping Using Remote Sensing and Weather Datasets: A New Parameterization for the SSEB Approach. *J. Am. Water Resour. Assoc.* **2013**, *49*, 577–591.
31. Senay, G.B.; Budde, M.; Verdin, J.P.; Melesse, A.M. A coupled remote sensing and simplified surface energy balance approach to estimate actual evapotranspiration from irrigated fields. *Sensors* **2007**, *7*, 979–1000.
32. Huffman, G.J.; Adler, R.F.; Stocker, E.; Bolvin, D.T.; Nelkin, E.J. Analysis of TRMM 3-Hourly Multi-Satellite Precipitation Estimates Computed in Both Real and Post-Real Time. In Proceedings of the 12th Conference on Satellite Meteorology and Oceanography, Long Beach, CA, USA, 8–13 February 2003; pp. 9–13.
33. NASA-GSFC Tropical Rainfall Measuring Mission (TRMM). Available online: http://trmm.gsfc.nasa.gov/data_dir/data.html (accessed on 6 July 2013).
34. McLeod, A.I. Kendall: Kendall Rank Correlation and Mann-Kendall Trend Test, R Package Version 2.2; 2011. Available online: <http://CRAN.R-project.org/package=Kendall> (accessed on 19 February 2015).
35. De Beurs, K.; Henebry, G. Trend analysis of the Pathfinder AVHRR Land (PAL) NDVI data for the deserts of central Asia. *Geosci. Remote Sens. Lett. IEEE* **2004**, *1*, 282–286.
36. De Beurs, K.M.; Henebry, G.M. A statistical framework for the analysis of long image time series. *Int. J. Remote Sens.* **2005**, *26*, 1551–1573.
37. R Development Core Team. *R: A Language and Environment for Statistical Computing*; R Foundation for Statistical Computing: Vienna, Austria, 2014.
38. Boschetti, M.; Nutini, F.; Brivio, P.A.; Bartholomé, E.; Stroppiana, D.; Hoscilo, A. Identification of environmental anomaly hot spots in West Africa from time series of NDVI and rainfall. *ISPRS J. Photogramm. Remote Sens.* **2013**, *78*, 26–40.
39. Tucker, C.J.; Vanpraet, C.L.; Sharman, M.J.; van Ittersum, G. Satellite remote sensing of total herbaceous biomass production in the Senegalese Sahel: 1980–1984. *Remote Sens. Environ.* **1985**, *17*, 233–249.
40. Nemani, R.R.; Keeling, C.D.; Hashimoto, H.; Jolly, W.M.; Piper, S.C.; Tucker, C.J.; Myneni, R.B.; Running, S.W. Climate-driven increases in global terrestrial net primary production from 1982 to 1999. *Science* **2003**, *300*, 1560–1563.
41. Karajeh, F.; Oweis, T.; Swelam, A.; El-Gindy, A.-G.; El-Quosy, D.E.D.; Khalifa, H.; El-Kholy, M.; El-Hafez, S.A.A. *Water and Agriculture in Egypt*; International Center for Agricultural Research in the Dry Areas (ICARDA): Beirut, Lebanon, 2011.
42. Gersfelt, B. Allocating Irrigation Water in Egypt. In *Food Policy for Developing Countries: Case Studies*; Pinstrip-Andersen, P., Cheng, F., Eds.; Cornell University Library: Ithaca, NY, USA, 2007; p. 14.

43. Wichelns, D.; Qadir, M. Achieving sustainable irrigation requires effective management of salts, soil salinity, and shallow groundwater. *Agric. Water Manag.* **2015**, *157*, 31–38.
44. El Baroudy, A.A.; Moghanm, F.S. Combined use of remote sensing and GIS for degradation risk assessment in some soils of the Northern Nile Delta, Egypt. *Egypt J. Remote Sens. Space Sci.* **2014**, *17*, 77–85.
45. Barnes, J. Mixing waters: The reuse of agricultural drainage water in Egypt. *Geoforum* **2014**, *57*, 181–191.
46. Hassanein, M.; Fahim, M.; Khalil, A.; Abolmaty, S.; Refaie, K.; Taqi, M.; Abou Hadid, A. Impact of urbanization on agricultural land losses and climate change Case study: Gharbiah Governorate, Egypt. *J. Am. Sci.* **2014**, *10*, 99–107.
47. Khalil, A.; Essa, Y.; Hassanein, M. Monitoring Agricultural Land Degradation in Egypt Using MODIS NDVI Satellite Images. *Nat. Sci.* **2014**, *12*, 15–21,
48. Bakr, N.; Weindorf, D.; Bahnassy, M.; Marei, S.; El-Badawi, M. Monitoring land cover changes in a newly reclaimed area of Egypt using multi-temporal Landsat data. *Appl. Geogr.* **2010**, *30*, 592–605.
49. El-Shirbeny, M.A.; Aboelghar, M.A.; Arafat, S.M.; El-Gindy, A.-G.M. Assessment of the mutual impact between climate and vegetation cover using NOAA-AVHRR and Landsat data in Egypt. *Arab. J. Geosci.* **2014**, *7*, 1287–1296.
50. Abd El-Kawy, O.R.; Rød, J.K.; Ismail, H.A.; Suliman, A.S. Land use and land cover change detection in the western Nile Delta of Egypt using remote sensing data. *Appl. Geogr.* **2011**, *31*, 483–494.
51. Johnston, R. Availability of water for agriculture in the Nile Basin. In *The Nile River Basin, Water, Agriculture, Governance and Livelihoods*; Awulachew, S.B., Smakhtin, V., Molden, D., Peden, D., Eds.; Routledge-Earthscan: Abingdon, UK, 2012; pp. 61–83.
52. Mengistu, D.; Bewket, W.; Lal, R. Recent spatiotemporal temperature and rainfall variability and trends over the Upper Blue Nile River Basin, Ethiopia. *Int. J. Clim.* **2014**, *34*, 2278–2292.
53. Tesemma, Z.K.; Mohamed, Y.A.; Steenhuis, T.S. Trends in rainfall and runoff in the Blue Nile Basin: 1964–2003. *Hydrol. Process.* **2010**, *24*, 3747–3758.
54. Senay, G.B.; Asante, K.; Artan, G. Water balance dynamics in the Nile Basin. *Hydrol. Process.* **2009**, *23*, 3675–3681.